Nanostructure and Bioactivity of Hybrid Aerogels

Antonio J. Salinas,*,† María Vallet-Regí,*,† José A. Toledo-Fernández,‡ Roberto Mendoza-Serna,‡ Manuel Piñero,§ Luis Esquivias,|| Julio Ramírez-Castellanos,⊥ and José M. González-Calbet⊥

Departamento Química Inorgánica y Bioinorgánica, Facultad de Farmacia, Universidad Complutense, 28040 Madrid, Spain, Departamento Física de la Materia Condensada, Facultad de Ciencias, Universidad de Cádiz, Puerto Real 11510 Cádiz, Spain, Departamento Física Aplicada, CASEM, Universidad de Cádiz, Puerto Real E-11510 Cádiz, Spain, Departamento Física Materia Condensada, Facultad de Físicas, Universidad de Sevilla, 41012 Sevilla, Spain, and Departamento Química Inorgánica, Facultad C.C. Químicas, Universidad Complutense, 28040 Madrid, Spain

Received February 21, 2008. Revised Manuscript Received November 6, 2008

Hybrid sono-aerogels in the $CaO-SiO_2$–poly(dimethyl siloxane) (PDMS) system with low density and high surface area and pore volume were investigated to be used as biomaterials. Their in vitro bioactivity was monitored by soaking in a simulated body fluid (SBF). All the aerogels exhibited similar wetting and dissolution properties, but only the aerogel of composition 20 wt % PDMS–20 wt % CaO (S20Ca20) exhibited a bioactive response in SBF. To investigate the relationship between the different in vitro behaviours and the hybrids nanostructure, samples were studied by high-resolution transmission electron microscopy (HRTEM). All the aerogels showed similar basic microstructural features exhibiting amorphous Ca-free areas characterized by Si–O–Si distances of 0.23 nm. However, crystallized nanodomains containing calcium were also detected in S20Ca20. These domains, identified as pseudowollastonite and other Ca–Si–O phases, could explain the bioactive response of this material. Bioactivity and good textural and mechanical properties turn S20Ca20 aerogel into a candidate as biomaterial.

Introduction

The search of new bioactive materials with well-defined porosity is an important goal in the Biomaterials field.[1−4] The term "bioactive" was coined for materials that bond with the living tissues when implanted. However, currently it is also commonly used for materials coated by an apatite-like layer in vitro, that is, after being soaked in solutions mimicking blood plasma.[5−7] The reason is because this layer should facilitate, under in vivo conditions, interaction with biological entities, initiating a sequence of reactions producing new bone that bonds the material to the living tissues.[6] Besides bioactivity, hierarchical porosity is also necessary for a new biomaterial.[8] Several decades ago, an important role was suggested for interconnected pores greater than 100 μm in size to ensure cell colonization and tissue vascularisation, as well as the morphological fixation of prosthesis.[6] More recently, the need has been established for pores in the nanometers range able to host and release, in a controlled way, substances inducing the regeneration of living tissues.[2,3]

In 1997, Tsuru et al. proposed the synthesis of organic–inorganic hybrids to produce new bioactive materials with improved properties.[9] In these materials the inorganic component ensures bioactivity, whereas the organic polymer permits tailoring of the mechanical properties,[10−12] and degradation behavior,[13,14] and to include certain functional groups with specific interactions with biological entities.[15] In the search of new biomaterials for clinical applications that require low-density bioactive monoliths with high pore volume, for instance, for small bone prosthesis, the synthesis of organic–inorganic hybrid aerogels could be a suitable approach.

In this paper, the synthesis and characterization of new hybrid aerogels in the $CaO-SiO_2$–poly(dimethyl siloxane) (PDMS) system is described. To increase the uniformity of

* Corresponding author. Ph. 34 91 3941790. Fax: 34 91 3941786. E-mail: salinas@farm.ucm.es (A.J.S.); vallet@farm.ucm.es (M.V.-R.).
† Departamento Química Inorgánica y Bioinorgánica, Universidad Complutense.
‡ Departamento Física de la Materia Condensada, Universidad de Cádiz.
§ Departamento Física Aplicada, Universidad de Cádiz.
|| Departamento de Física de la Materia Condensada, Universidad de Sevilla.
⊥ Departamento Química Inorgánica, Universidad Complutense.

(1) Vallet-Regi, M. *J. Chem. Soc., Dalton Trans.* **2001**, 97.
(2) Vallet-Regi, M. *Dalton Trans.* **2006**, 5211.
(3) Vallet-Regi, M. *Chem.–Eur. J.* **2006**, *12*, 5934.
(4) Salinas, A. J.; Vallet-Regi, M. *Z. Anorg. Allg. Chem.* **2007**, 1762.
(5) Kokubo, T.; Kushitani, H.; Sakka, S.; Kitsugi, T.; Yamamuro, T. *J. Biomed. Mater. Res.* **1990**, *24*, 721.
(6) Hench, L. L. *J. Am. Ceram. Soc.* **1991**, *74*, 1487.
(7) Vallet-Regi, M.; Ragel, C. V.; Salinas, A. J. *Eur. J. Inorg. Chem.* **2003**, 1029.
(8) Hench, L. L.; Polack, J. M. *Science* **2002**, *295*, 1014.
(9) Tsuru, K.; Ohtsuki, C.; Osaka, A.; Iwamoto, T.; Mackenzie, J. D. *J. Mater. Sci: Mater. Med.* **1997**, *8*, 157.
(10) Chen, Q.; Miyaji, F.; Kokubo, T.; Nakamura, T. *Biomaterials* **1999**, *20*, 1127.
(11) Kamitakahara, M.; Kawashita, M.; Miyata, N.; Kokubo, T. *J. Mater. Sci: Mater. Med.* **2003**, *14*, 1067.
(12) Salinas, A. J.; Merino, J. M.; Gil, F. J.; Babonneau, F.; Vallet-Regi, M. *J. Biomed. Mater. Res. B* **2007**, *81B*, 274.
(13) Pereira, A. P. V.; Vasconcelos, W. L.; Orefice, R. K. *J. Non-Cryst. Solids* **2000**, *273*, 180.
(14) Martin, A. I.; Salinas, A. J.; Vallet-Regi, M. *J. Eur. Ceram. Soc.* **2005**, *25*, 3533.
(15) Colilla, M.; Salinas, A. J.; Vallet-Regi, M. *Chem. Mater.* **2006**, *18*, 5676.

10.1021/cm800511r CCC: $40.75
Published on Web 12/03/2008

particles and pore size, precursor sol preparation was carried out with high powder ultrasound assistance in the absence of an added solvent. To prevent materials shrinkage and obtain low-density materials, drying was performed under supercritical conditions. The in vitro behavior of these sono-aerogels was studied in Kokubo's Simulated Body Fluid (SBF).[5] To investigate the nanostructural basis of bioactivity, we characterized sono-aerogels by high-resolution transmission electron microscopy (HRTEM).

Experimental Section

Sample Preparation. Hybrid organic−inorganic silica gels were synthesized by the sol−gel method by means a two-step procedure. In the first step, 0.0223 mol of TEOS (tetraethoxysilane, Aldrich), used as source for silica inorganic phase, were partially hydrolyzed understoichiometrically with water acidified to pH 0 with HNO_3 (Panreac, 60%) in a molar ratio of TEOS:H_2O of 1:0.84; then silanol-terminated PDMS with quoted average molecular weight of 400−700 g/mol (ABCR, USA; 99.5%) was added as the organic component as a required wt % of the total silica content, depending on the desired hybrid composition. In this study aerogels containing between 10 and 50 wt % PDMS were prepared. At this stage, 640 J cm^{-3} of ultrasound was applied during 12 min to the mix from a device delivering 0.6 w cm^{-3} of ultrasound power energy to the system, resulting in a transparent and homogeneous solution that was kept at 50 °C for 24 h. In a second step, 0.41 mol of HNO_3 catalyst in a 1 M water solution was added to complete the hydrolysis reaction with a molar ratio TEOS:H_2O of 1:3.16 and supplying 320 J cm^{-3} ultrasound energy during 12 min. Then, calcium nitrate [$Ca(NO_3)_2 \cdot 4H_2O$] (Fluka), as phase for inducing bioactivity, was added at a level of 10 or 20 wt % of the total silica with an additional application during 12 min of 320 J cm^{-3} ultrasound energy, representing a total of 1280 J cm^{-3}.

The liquid sol was kept in hermetically close container up to gelation took place. Further, the resulting gel was washed in an extra volume of ethanol (0.034 mol in all the cases), expelling the residual water from the pores. It was left for 24 h, under which conditions calcium ions were not removed into the ethanol.

Finally, the gel was placed into an autoclave and the pore liquor was vented off above the supercritical conditions of ethanol (243 °C, 63 bar). The supercritical state was attained by slow heating (1 °C/min) to minimize the effect of the thermal expansion of ethanol, which is much greater than that of the wet silica gel network. Heating results in the evaporation of the additional volume of ethanol that permits the supercritical temperature and pressure (255 °C, 85 bar) to be reached without crossing the vapor−liquid equilibrium curve, avoiding capillary pressures on the adjacent pores. In this way, the structure does not collapse and the aerogel retains its original microstructure. Test samples were thereby made as crack-free cylinders 18 mm long and 8 mm diameter suitable for measurement of mechanical properties and bioactivity. Density was calculated by weighing samples with a well defined geometry.

Aerogel Nomenclature. $CaO-SiO_2$−PDMS samples were denoted as S*x*Ca*y* where "*x*" is the wt % organic polymer with respect to silica and "*y*" designates the corresponding wt % calcium expressed as the oxide. (e.g., S50Ca10 represents an aerogel that contains 50 wt % PDMS and 10 wt % CaO with respect to the total silica in the gel).

Characterization of Aerogels. Samples were characterized by thermogravimetric (TG) and differential thermogravimetric (DTG) analyses in air at 10 °C min^{-1} heating rate, from 25 to 1000 °C in a Setaram Setsys 1750. N_2 porosimetry was performed in a Sorptomatic 1990 (CE Instruments) equipment. From the N_2 adsorption/desorption isotherms, the BET specific surface areas were obtained.[16] The corresponding average pore diameter was evaluated using the BJH method.[17] Wetting was measured in Rame−Hart contact angle goniometer using the sessile drop method. Solid-state ^{29}Si magic angle spinning nuclear magnetic resonance (^{29}Si MAS NMR) spectra were obtained on a Bruker Avance AV-400WB spectrometer (400 MHz). The spectrometer frequency was set to 79.49 MHz and the chemical shift values were referenced at 0 ppm to 3-(trimethylsilyl)-1-propanesulfonic acid sodium salt (DSS sodium salt). The samples were packed into a zirconia rotor spinning at 10 kHz and the spectra were recorded using a 5 s recycle delay and a pulse wide of 4.5 μs; the number of scans was 10 000. Mechanical tests were performed in an AG-I Autograph from Shimadzu, equipped with a load cell of 5 kN, by means of uniaxial compression. All the experiments were performed at room temperature, with a fixed strain rate of 0.5 mm/s.

In vitro Bioactivity. Assessment of the in vitro bioactivity was carried out by soaking cylindrical pieces of aerogel (8 mm diameter, 3 mm in height) for times up to 28 days in simulated body fluid (SBF) at 37 °C.[5] SBF is an acellular aqueous solution with an inorganic ion composition almost equal to human plasma: Na^+, 142; K^+, 5.0; Mg^{2+}, 1.5; Ca^{2+}, 2.5; Cl^-, 147.8; HCO_3^-, 4.2; HPO_4^{2-}, 1.0; and SO_4^{2-}, 0.5 mM, buffered at pH 7.40 with tris(hydroxymethyl) aminomethane/HCl. After being soaked, the pieces were removed from SBF, lightly rinsed in water and acetone and allowed to air-dry at room temperature. To avoid contamination by microorganisms, we performed all manipulations/operations in a laminar flux cabinet Telstar AV-100 and filtered the SBF with a 0.22 μm Millipore system before the in vitro assays. Dissolution of samples was quantified by measuring the ionic variations in SBF with an ion selective electrode ILyte analyzer. Before and after the SBF treatments, samples were analyzed by Fourier transform infrared (FTIR) spectroscopy, in a Nicolet Nexus spectrometer equipped with a diamond ATR Goldengate, scanning electron microscopy (SEM), and energy-dispersive X-ray spectroscopy (EDS), in a JEOL 6400 Microscope equipped with an Oxford-LINK Pentafet System. In general, materials coated by an apatite-like layer after being soaked in SBF are categorized as bioactive, whereas when the surface remained unchanged after the SBF treatment, they are considered as nonbioactive.

Aerogel Nanostructure. The nanostructure of as prepared sono-aerogels was studied by selected area electron diffraction (SAED) and high-resolution transmission electron microscopy (HRTEM) in a JEOL 300 FEG electron microscope. Inverse fast Fourier transform (IFFT) images were obtained from HRTEM images by windowing the Fast Fourier Transform (FFT) patterns. EDS studies were also performed in this microscope with an Oxford model ISIS analyzer.

Results and Discussion

Aerogel Characterization. TG and DTG results obtained for S50Ca10 aerogel are presented in Figure 1. The first weight loss (∼2%) at 80−100 °C, can be assigned to the elimination of H_2O and residual solvent. The second weight loss (∼10%) in the 220−250 °C interval can be attributed to the combustion of the PDMS in the hybrids. The third weight loss, at 390−425 °C (∼10%), corresponds to the decomposition of the remaining nitrate groups after the supercritical drying to obtain the aerogels. After that, a

(16) Brunauer, S.; Emmet, P. H.; Teller, E. *J. Am. Chem. Soc.* **1938**, *60*, 309.
(17) Barret, E. P.; Joyner, L. G.; Halenda, P. P. *J. Am. Chem. Soc.* **1951**, *73*, 373.

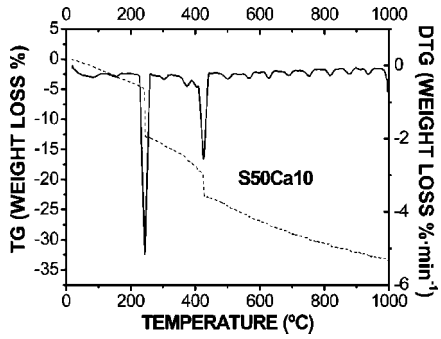

Figure 1. TG and DTG results of S50Ca10.

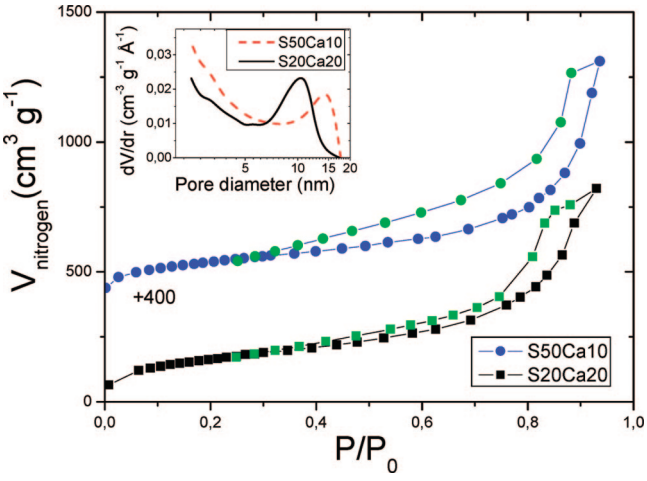

Figure 2. N_2 adsorption−desorption isotherms of S20Ca20 and S50Ca10. Inset: pore diameter distributions from BJH model on the desorption branch.

Table 1. Textural Properties of Several Hybrid Sono-Aerogels

aerogel	PDMS (%)	CaO (%)	S_{BET} (m^2 g^{-1})	avg D_P (nm)
S20Ca0	20	0	1283	3.0
S20Ca10	20	10	776	3.2
S20Ca20	20	20	599	11.1
S40Ca20	40	20	537	15.6
S10Ca10	10	10	1096	9.6
S30Ca10	30	10	929	10.5
S50Ca10	50	10	511	15.2

continuous weight loss took place until a total value of 32.5% for this sample. All the aerogels of this series gave similar TG traces (results not shown) with different weight loss values in each interval depending on the PDMS and calcium nitrate contents in the material.

Figure 2 shows the nitrogen adsorption−desorption isotherms at 77 K for S50Ca10 and S20Ca20, selected as representative examples of the complete series. According to the IUPAC classification, these are Type IV isotherms, which appears in porous adsorbents containing pores whose diameters are in the range 2−200 nm. The N_2 adsorption at low pressure is produced by the formation of multiple layers. At high pressure, the adsorption is caused by capillary condensation, which is characterized by a clear hysteresis loop occurring in the mesoporous range (2−50 nm). An apparent linear region in BET plot up to $P/P_0 = 0.35$ gives the specific surface area (S_{BET}). In Table 1 are presented textural parameters of several sono-aerogels compositions. As observed, for identical PDMS contents, when the calcium increases, S_{BET} and the average pore diameter (D_P) decrease. On the other hand, for constant calcium content, S_{BET} and D_P increase with increasing PDMS content.

Focusing on the samples for which isotherms are plotted in Figure 2, the surface area of S50Ca10 smaller than that of S20Ca20 is a consequence of its higher polymer content; given that the inorganic phase contributes in a more extent to the specific surface area.[18] This fact seems to be contradictory with the pore volume values, 1.41 cm^3 g^{-1} for S50Ca10 and 1.27 cm^3 g^{-1} for S20Ca20, but such an event must be related with the smaller inorganic content that give a lesser bulk density (0.54 against 0.58 g cm^{-3}, for S50Ca10 and S20Ca20, respectively). The pore diameter values and the t-plot analysis (results not shown) indicate some microporous contribution in the case of S20Ca20 with more amount of inorganic phase. In general, microporosity is a characteristic of silica aerogels from sols prepared with high-powder ultrasound assistance in the absence of an added solvent.[19,20] This is modified by the presence of the organic phase. In fact, the isotherms in Figure 2 do not show a completely linear behavior at low pressure: there is a slight increase in adsorbed volume at $P/P_0 < 0.04$, typical of microporous solids. Also, the extent of the hysteresis loop indicates a very slow desorption of N_2 in the low P/P_0 region. This corroborates the conclusion that a few micropores remain in the matrix of the inorganic phase.

On the other hand, the isotherms show hysteresis loop classified as H1 type, in which it exhibits parallel and near vertical branches on the high relative pressure side, but condensation and evaporation in pores occur at different relative pressure. This kind of hysteresis loops is often reported for materials that consisted of agglomerates (assemblages of rigidly joint particles) or compacts of approximately spherical particles arranged in a fairly uniform way, as in this case achieve the $CaSiO_3$ pseudowollastonite particles. Hence, the appearance of the H1 hysteresis loop on the isotherm for a mesoporous solid generally indicates high pore size uniformity and pore interconnectivity.[21,22] The agreement of our results with the above discussion are apparent by the pore size distribution showed in the inset of Figure 2, giving that they were calculated from the BJH method. Pore interconnectivity and size uniformity are major characteristics to obtain an efficient bioactivity performance and to use these materials for hosting and releasing, in a controlled way, molecules with biological activity.

Thus, the combined effect of high-power ultrasound and the absence of an added solvent in the liquid state during the synthesis gave rise to a gel made up of small and uniformly sized particles and pores. As a consequence, the surface/volume ratio is twice as large as that for gels prepared in an alcoholic solution.[19] The dense, cross-linked wet "sonogels" are dried under supercritical conditions to prevent any shrinkage, resulting in an aerogel whose density is

(18) Santos, A.; Toledo-Fernández, J. A.; Mendoza-Serna, R.; Gago-Duport, L.; de la Rosa-Fox, N.; Pïnero, M.; Esquivias, L. *Ind. Eng. Chem. Res.* **2007**, *46*, 103.
(19) De la Rosa-Fox, N.; Esquivias, L.; Craievich, A.; Zarzycki, J. *J. Non-Cryst. Solids* **1990**, *121*, 211.
(20) De la Rosa-Fox, N.; Esquivias, L.; Zarzycki, J. *Diffus. Defect Data* **1987**, *53&54*, 363.
(21) Kruk, M.; Jaroniec, M.; Sayari, A. *Langmuir* **1997**, *13*, 6267.
(22) Kruk, M.; Jaroniec, M. *Chem. Mater.* **2001**, *13*, 3169.

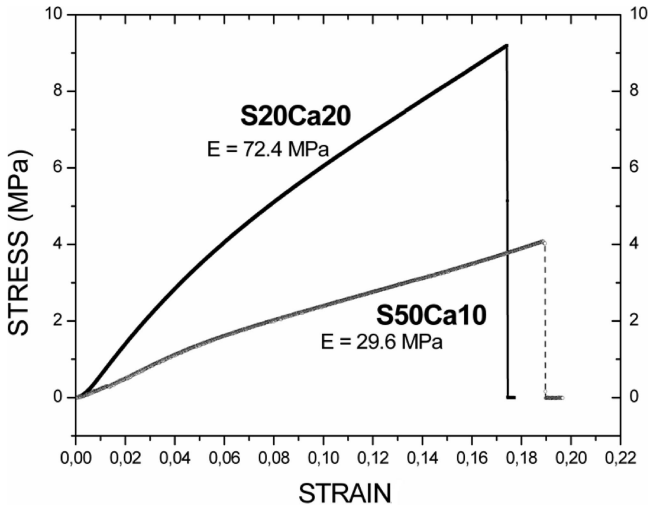

Figure 3. Stress−strain curves of S20Ca20 and S50Ca10. Young's modulus values, *E*, are also included.

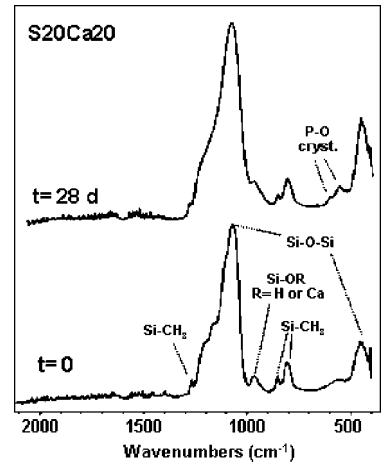

Figure 4. FTIR spectra of S20Ca20 before and after soaking 28 days in SBF. The bands around 600 cm^{-1} suggest the presence of phosphate groups in a crystalline environment.

40−50% that of vitreous silica (2.2 g cm^{-3}), whereas the density of classic aerogels is only 10−20% of that density.[20] The higher density of sonogels could improve their mechanical properties.

Figure 3 shows the standard stress−strain curves for S20Ca20 and S50Ca10 aerogels under uniaxial compression. A first linear region up to 4% strain gives an elastic modulus of 72.4 MPa for S20Ca20, at the low end of the cancelous human bone (50−500 MPa).[23] For the S50Ca10 sample, the elastic modulus diminishes at 29.6 MPa. The slope change can be attributed to the pore collapse and not to a plastic behavior. It must take into account that the incorporation of organic polymer chains into the inorganic structure dramatically changes the mechanical behavior of these materials. That way, for organic contents greater than 20% by weight, these materials has an elastomeric behavior. As the stress increases, the PDMS aerogel begins to deform less and less, indicating that the solid network is becoming stiffer; the action of the polymer then stops and the inorganic silica network begins to act, and ends with a similar slope (elastic modulus) as the pure silica aerogel.[24,25] For the samples in Figure 2, the strain at rupture occurred at 17% for S20Ca20 and 19% for S50Ca10, respectively, and the corresponding stresses were 9 and 4 MPa. Aerogels with lower PDMS content, i.e., S10Ca0 and S10Ca50, exhibited higher elastic moduli of 87 and 74 MPa, respectively, with stresses to rupture of 7.8 and 9.3 MPa at deformations of 12 and 17%, respectively.

Bioactivity Assays. The in vitro behavior of hybrid aerogels was monitored by soaking pieces of each composition in SBF and analyzing the changes in their surfaces by FTIR, SEM and EDS. After 7 days of immersion, some new material started to be formed on S20Ca20 and by 28 days, the pieces appeared fully covered by a newly formed layer. However, in all the remaining aerogels synthesized, even after 28 days of soaking, their surfaces continue unchanged, indicating that these hybrid materials do not present an in vitro bioactive response.

Figure 4 shows the FTIR spectra of S20Ca20 aerogel before and after being soaked 28 days in SBF. The spectrum of the untreated hybrid ($t = 0$) shows bands at 1040 and 440 cm^{-1}, that can be assigned to Si−O−Si normal vibration modes, and bands at 1263, 848, and 802 cm^{-1} of Si-CH_3 modes. After 28 days, the FTIR spectrum is somewhat similar, but new bands at 563 and 602 cm^{-1} are now present. These bands can be assigned to O−P−O bending modes in a crystalline environment,[26] suggesting a positive in vitro bioactive response for this aerogel.

To confirm the calcium phosphate-rich layer formation, the S20Ca20 surface was studied by SEM and EDS. In Figure 5, the SEM images and the EDS spectra for S20Ca20 aerogel before and after 28 days in SBF are shown. Before immersion, a smooth surface composed of silicon, calcium and oxygen is observed (Figure 5a). However, after 28 days soaked, the aerogel surface appeared covered by a new material formed by globular agglomerates of flake-like particles (Figure 5b), more visible in the micrograph at higher magnification (Figure 5c). In addition, by tilting the sample a layer thickness close to 5 μm was observed (Figure 5d). Such thick layers are only detected in materials with relatively high bioactive response. The correspondent EDS spectra show that the layer is mainly composed of Ca and P in a Ca/P molar ratio of 1.37. This low value, far from stoichiometric hydroxyapatite (1.67) or calcium deficient apatite (around 1.50), suggests that the main phase in the layer could be the apatitic octacalcium phosphate (Ca/P = 1.33) considered as precursor of the calcium deficient apatite. Another fact supporting the majority presence of octacalcium phosphate in the layer is the absence of the bands of carbonate groups in Figure 4 that would be present if carbonated calcium deficient apatite was formed. Furthermore, the EDS analysis of the soaked sample reveals the presence in the layer of small amounts of Cl^-, Na^+, and Mg^{2+}

(23) Wan, X. H.; Chang, C. K.; Mao, D. L.; Jiang, L.; Li, M. *Mater. Sci. Eng., C* **2005**, *25*, 455.
(24) Zarzycki, J. *J. Non-Cryst. Solids* **1988**, *100*, 359.
(25) De la Rosa-Fox, N.; Morales-Flórez, V.; Piñero, M.; Esquivias, L. *Key Eng. Mater.* **2009**, *391*, 45, available on-line at, doi:10.4028/0−87849−365−4.45.
(26) Elliott, J. C. *Structure and Chemistry of the Apatites and Other Calcium Orthophosphates*; Elsevier: London, 1994; p 59.

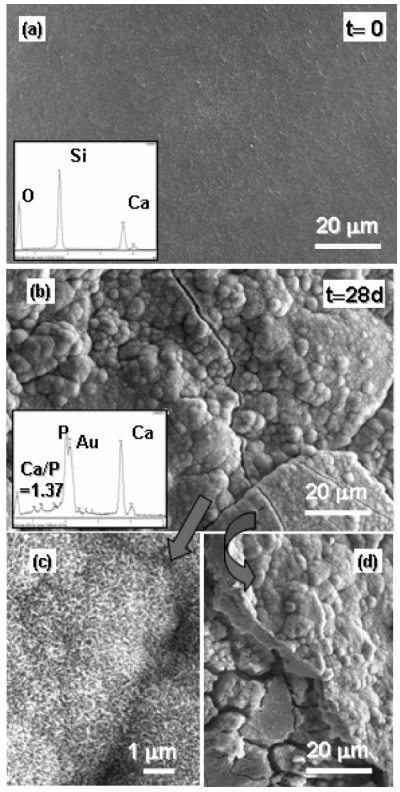

Figure 5. SEM micrographs and EDS spectra of S20Ca20: (a) before and (b) after 28 days soaking in SBF. (c, d) EDS micrographs at higher magnification and tilting the sample to see the layer thickness, respectively.

ions, very abundant in the SBF solution, which could indicate the coprecipitation of small amounts of these salts and/or their inclusion in the apatite-like structure.

Therefore, the FTIR spectroscopy in conjunction with SEM and EDS analyses has indicated an in vitro bioactive response of S20Ca20, which suggests that this organic−inorganic hybrid aerogel is of interest as a biomaterial. However, the other compositions studied do not present a bioactive response. To explain why S20Ca20 was the only aerogel presenting a bioactive response, wetting and dissolution studies were performed. It would be possible to speculate that S20Ca20, relatively low in PDMS and high in CaO, could present high water affinity and released abundant Ca^{2+} ions to solution, which could explain its positive bioactive response. However, S20Ca20 presented similar wetting and dissolution properties to non-bioactive hybrids. For instance, the contact angle with water was 145° for S20Ca20 and 143° for nonbioactive S50Ca10. Other aerogels, like S30Ca10 and S10Ca10, exhibited contact angles close to 135° but, in spite of this higher water affinity, they were not bioactive.

With respect to the dissolution of hybrids we focused *o*n the initial period of immersion to avoid possible interfering precipitation processes from solution. After 24 h, all the aerogels followed analogous trends with minimum increases of $[Ca^{2+}]$ in solution from 2.46 to 2.54 mM and pH from 7.33 to 7.34. So small variations in the ionic composition of solution were identical for all the aerogels, including bioactive S20Ca20 and not bioactive S50Ca10, S30Ca10, and S10Ca10. For comparison, after 24 h of soaking,

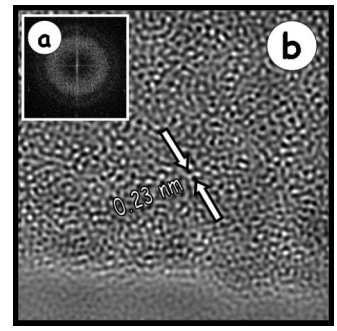

Figure 6. (a) Diffused scattering and rings at low angles observed in the FFT pattern of the S50Ca10 sample indicate an amorphous microstructure, as seen in (b) the corresponding IFFT image.

bioactive $CaO-SiO_2$ sol−gel glasses undergo substantial increases of $[Ca^{2+}]$ and pH up to 9.0 mM and 7.7, respectively.[7] Therefore, it seems that causes other than wetting or dissolution must be responsible for the in vitro bioactive response of S20Ca20.

^{29}Si NMR measurements of the hybrids did not show special features of S20Ca20 that could explain its bioactive response. For instance, the percentage of Q_3 and Q_2 species, often considered as responsible of bioactivity, were similar for S20Ca20, 41 and 4%, respectively, and nonbioactive hybrids such as S50Ca10 or S10Ca10. Finally, the nanostructural features of aerogels were studied by HRTEM. For clarity, only data from bioactive S20Ca20 and nonbioactive S50Ca10 will be presented. Similar results to S50Ca10 were obtained for the remaining nonbioactive hybrids.

Nanostructural Characterization of Sono-Aerogels. All the hybrid aerogels of this system show similar basic microstructural features. Figure 6a shows the FFT pattern corresponding to the S50Ca10 sample, which is obtained from the digitized experimental HRTEM image. Broad diffused scattering and rings at low angles indicate the amorphous nature of the sample. By applying a mask around all the fundamental spots in the FFT pattern, high-frequency nonperiodic noise is strongly suppressed, and a subsequent inverse Fourier transformation (IFFT) image is obtained, leading to a clearer image with stronger contrasts. In the corresponding obtained IFFT image (Figure 6b), the typical contrast of an amorphous material is seen. The projected potential of a crystal depends mainly on the species of the component elements. The electrostatic potential in a crystal composed of light elements is generally low. On the other hand, the columns along which heavy atoms densely array are seen as dark spots. Because the image contrast is proportional to the projected potential, it is possible to discriminate the atomic species. On the basis of this information, it can be assumed that dots observed in Figure 6b are correlated with the positions of tetrahedral $[SiO_4^{4-}]$ units, as previously reported by Vallet-Regí et al.[27] An average distance between these strong contrasts of 0.23 nm is measured, which can correspond to the Si−O−Si distance.

Moreover, in the S20Ca20 sample, some different microstructural features were found. As can be observed, the intensity and discrete spots (indicated by arrows) in this FFT

(27) Vallet-Regi, M.; Salinas, A. J.; Ramirez-Castellanos, J.; Gonzalez-Calbet, J. M. *Chem. Mater.* **2005**, *17*, 1874.

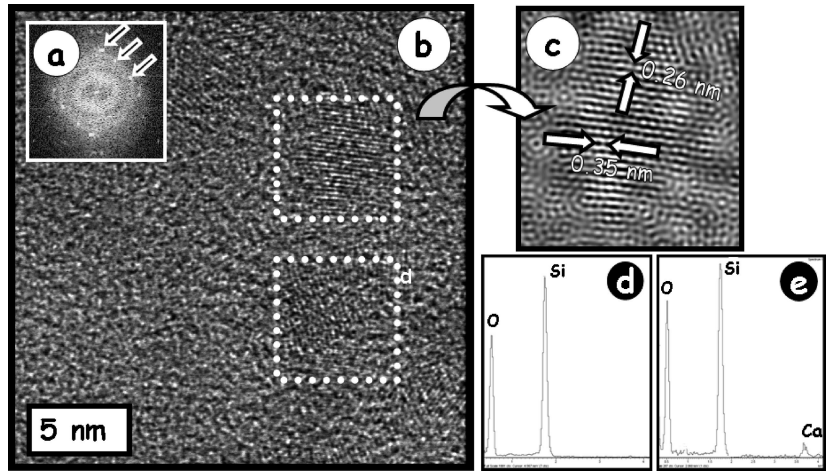

Figure 7. (a) FFT pattern of S20Ca20 showing discrete spots (indicated by arrows) and diffused rings at low angles, suggesting the presence of randomly oriented grains as observed in (b) the corresponding micrograph, where the glassy matrix contains some poorly crystallized domains (dashed square), clearly seen in (c) the enlarged image. EDS microanalysis corresponding to (d) amorphous areas and (e) ordered areas are shown. IFFT image (b).

pattern (Figure 7a) suggest the presence of randomly oriented grains of very small dimensions. FFT patterns also present broad diffused scattering, as well as diffused rings at low angles, probably because of an amorphous nature of the sample. Figure 7b reveals a complex microstructure, where a glassy matrix containing some poorly crystallized domains (noted with a dashed square) are found. Average interplanar distances of 0.35 and 0.26 nm in the plane can be observed in the corresponding enlarged image (Figure 7c). EDS microanalysis confirms that amorphous areas contain Si but are Ca-free (Figure 7d). On the other hand, both Si and Ca are present in ordered areas (Figure 7e), suggesting that Ca incorporation gives rise to the formation of crystallization nuclei containing the Ca ions. Taking into account this information, the Si/Ca ratio determination is greatly affected by a matrix effect, because the crystallized domains are into a Si−O glassy matrix. Note that these microstructural features were not found in the previous S20Ca20 sample.

To identify the crystalline domains, we carried out a more detailed HRTEM study. Figure 8a shows the SAED pattern corresponding to a different area of the crystal, showing a pseudocubic projection where the strong spots (indicated by arrows) present streaking along both perpendicular directions, indicating the existence of some kind of structural disorder. In the corresponding HRTEM micrograph at low magnification (Figure 8b) areas with a high density of defects, as stacking faults and 90° twin boundaries, can be observed. Average interplanar distances close to 0.80 nm can be measured, corresponding to the *c*-axis of the $CaSiO_3$ pseudowollastonite type structure,[28] which can be described formed by a layer of ternary $[Si_3O_9]$ rings and a Ca-octahedral layer with lattice constants $a = 0.79$ nm, $b = 0.73$ nm, $c = 0.7.1$ nm; $\alpha = 103.43$, $\beta = 95.37$, and $\gamma = 90.03$) (Figure 9). Moreover, distances of 0.39 nm are clearly observed in the enlarged image along the perpendicular direction (Figure 10a), which is close to the Si···Si distance (0.31 nm) for ideal $[SiO_4^{4-}]$ tetrahedron in silicates, i.e., undistorted and/or undoped tetrahedron. However, as observed in the image, the spacings are far to be constant. A possible explanation of these observed *d*-spacings with respect to those of the stoichometric $CaSiO_3$ unit cell can

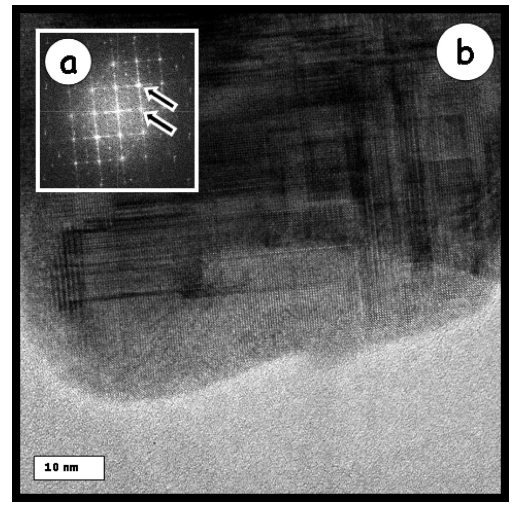

Figure 8. (a) SAED pattern of S20Ca20 shows a cubic symmetry projection where the strong spots (indicated by arrows) present streaking along both perpendicular directions. (b) Areas with a high density of defects can be observed in the corresponding HRTEM micrograph at low magnification.

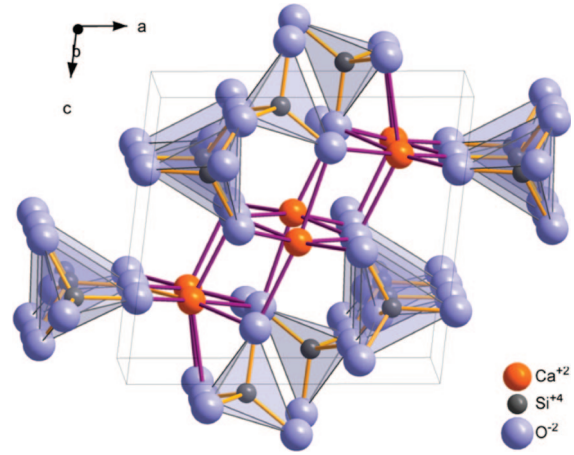

Figure 9. Unit cell of triclinic pseudowollastonite $CaSiO_3$.

(28) Buerger, M. J.; Prewitt, C. T. *Proc. Natl. Acad. Sci. U.S.A.* **1961**, *47*, 1884–1888.

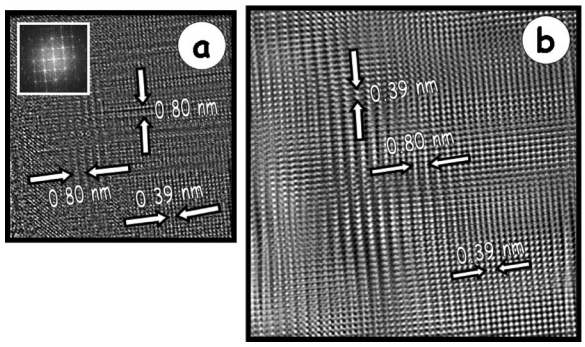

Figure 10. (a) Distances of 0.80 nm are clearly measured in the image of S20Ca20 along both perpendicular directions. However, the spacings are too far to be constant, as a consequence of disordered intergrowth along [001]. (b) Some areas completely free of such defects show lower periodicity.

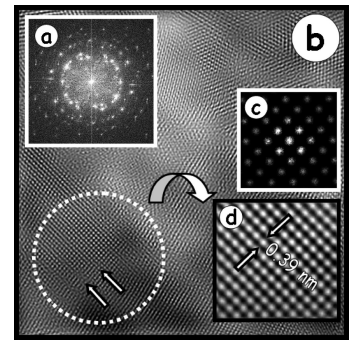

Figure 11. SAED pattern corresponding to another Ca-containing area of (a) S20Ca20, where some diffraction spots are observed, indicating the existence of small well crystallized domains (dashed circle), as observed in (b) the corresponding HRTEM image. (c) The corresponding FFT pattern along [001] zone axis is also shown. (d) Interplanar distances of 0.39 nm are measured in the corresponding enlarged micrograph.

be due to changes on the Ca/Si ratio in the obtained pseudowollastonite. Moreover, the observed HRTEM images present typical optical artifacts as a consequence of Moiré patterns due to the overlapping of crystallites. For his reason, the indicated spacings are average distances always keeping the ratio corresponding to the pseudowollastonite unit cell. A possible origin can reside in the disordered intergrowth along [001] of different silicates, in the same crystallographic orientation and in which different single, double and triple chains can be seen near the boundary.[29,30] In this sense, Hutchinson et al.[31] observed two types of stacking disorders, simple stacking faults and twinning, which also involves displacements in the composition planes. Both types of defects can produce new structures with different periodicities and spacings.

However, some areas are completely free of such defects, showing lower periodicity, with interplanar distances of 0.39 nm (Figure 10b). EDS microanalysis performed on this area confirms the presence of Si and Ca atoms, whereas only Si is observed in amorphous areas.

The SAED pattern of another Ca-containing area is depicted in Figure 11a, where some diffraction spots are clearly observed, indicating the existence of small well crystallized domains, as can be seen in the corresponding HRTEM image (Figure 11b). Particularly interesting is the very well ordered area shown at the bottom left (dashed circle), where a cubic structure is observed in this projection. Some structural disorder also exists (marked by black arrows). The corresponding FFT pattern along [001] zone axis is shown in Figure 11c. Interplanar distances of 0.39 nm (Figure 11d) are measured, which can correspond to the distance between two adjacent $[SiO_4^{4-}]$ tetrahedra, suggesting the existence of different $CaSiO_3$ polytypes, with a lower *c* parameter,[28] because the parameters defining the way in which individual tetrahedron are linked together are highly variable.[32] On the other hand, it is important to note that cubic $CaSiO_3$ phases can be stabilized under pressure. In this sense, we can take into account that our aerogels were obtained under hypercritical drying conditions, which can favor the stabilization of these phases. The EDS microanalysis performed on this area confirms the presence of Si and Ca.

Conclusions

The combined effect of high-power ultrasound and the absence of an added solvent gave rise to aerogels made up of small and uniformly sized particles and pores. The supercritical drying yields to materials with a density close to 0.5 g cm^{-3}.

Only S20Ca20 hybrid aerogel exhibited an in vitro bioactive response. Because this was the only one where $CaSiO_3$ nanocrystals were detected, such nanocrystals seem to be an essential requirement to reach in vitro bioactivity in $CaO-SiO_2-$PDMS aerogels.

Bioactivity and textural and mechanical properties of S20Ca20, surface area = 599 m^2 g^{-1}, pore volume = 1.27 cm^3 g^{-1}, and elastic modulus = 72.4 MPa, turn it into a good candidate for specific applications as biomaterial.

Acknowledgment. Financial support of CICYT (Spain) through research projects MAT2005-1486 and MAT2007-61927, Comunidad de Madrid through S-505-MAT-0324, and the European Union through FAME NoE, FP6-500159-1.

CM800511R

(29) Ingrin, J. *Phys. Chem. Miner.* **1993**, *20*, 56.
(30) Yamanaka, T.; Mori, H. *Acta Crystallogr., Sect. B* **1981**, *37*, 1010.
(31) Hutchison, J. L.; McLaren, A. C. *Contrib. Mineral. Petrol.* **1977**, *61*, 11–13.
(32) Mozzi, R. L.; Warren, B. E. *J. Appl. Crystallogr.* **1969**, *2*, 164.